Structural and Magnetic Properties of Oxidatively Stable Cobalt Nanoparticles Encapsulated in Graphite Shells

Michael A. Zalich,[†,§] Vincent V. Baranauskas,[§] Judy S. Riffle,[§] Martin Saunders,[‡] and Timothy G. St. Pierre*[,†]

School of Physics and Center for Microscopy and Microanalysis, The University of Western Australia, 35 Stirling Highway, Crawley, WA 6009, Australia, and Department of Chemistry and Macromolecules and Interfaces Institute, Virginia Polytechnic Institute and State University, Blacksburg, Virginia 24061

Received June 22, 2005. Revised Manuscript Received March 23, 2006

Oxidatively stable magnetic cobalt nanoparticles were prepared by annealing cobalt nanoparticles coated with poly(styrene-*b*-4-vinylphenoxyphthalonitrile) block copolymers. An oxygen-impermeable graphitic coating around the cobalt nanoparticles was created during thermal treatment at 700 °C owing to the thermal decomposition/cross-linking of a polymer with a highly aromatic character. A variety of analytical techniques were used to elucidate the physical properties of the pre-heat-treated and heat-treated samples. The cobalt-specific saturation magnetization (σ_s) increased from 81 to 173 emu g^{-1} Co upon heating of the polymer-coated cobalt nanoparticles. The pre-heat-treated sample readily oxidized, as revealed by low-temperature magnetic susceptometry studies, whereas the heat-treated sample showed oxidative stability for over 1 year. The mean cobalt particle size increased from 18.5 to 36.1 nm during thermal treatment. Electron diffraction and X-ray diffraction revealed that the pre-heat-treated particles were weakly crystalline, while the heat-treated particles were strongly crystalline. The dominant phase of the heat-treated sample was determined to be face-centered cubic with other minor phases present (hexagonal close packed and epsilon).

Introduction

Magnetic nanoparticles are of considerable interest owing to their potential applications in biomedicine and the magnetic recording industry, for example. There are several current and potential applications for magnetic nanomaterials in medicine including magnetic resonance imaging (MRI) contrast agents,[1] magnetic field directed drug delivery systems,[2,3] biotoxin removal,[4,5] gene therapy,[6,7] and magnetic fluid hyperthermia.[8] Iron oxides (magnetite and maghemite) have received much attention owing to their oxidative stability and biocompatibility; however, other transition metals and their alloys are also under investigation (Ni, Co, and Fe). Cobalt has one of the largest magnetic susceptibilities of these materials but it readily oxidizes upon exposure to air, resulting in the antiferromagnetic cobalt oxide. Hence, coating of cobalt nanoparticles with an oxygen-impermeable sheath is a necessary prerequisite for their potential use in biomedical applications.

Several research groups have prepared graphite-coated cobalt nanoparticles, nanorods, and nanocapsules utilizing the Krätschmer-Huffman carbon arc process designed for the

* To whom correspondence should be addressed: A/Prof. Timothy G. St. Pierre, School of Physics, The University of Western Australia, Crawley, WA, 6009, Australia. Tel.: +61 8 6488 2747. Fax: +61 8 6488 1879. E-mail: stpierre@physics.uwa.edu.au.

† School of Physics, The University of Western Australia.

‡ Center for Microscopy and Microanalysis, The University of Western Australia.

§ Virginia Polytechnic Institute and State University.

(1) Kohler, N.; Sun, C.; Wang, J.; Fryxell, G.; Zhang, M. In *Methotrexate Immobilized Superparamagnetic Nanoparticles for Cancer Diagnostics and Chemotherapeutics*, Fifth International Conference on the Scientific and Clinical Applications of Magnetic Carriers, Lyon, France, 2004; The Cleveland Clinic Foundation: Lyon, France, 2004; p 32.

(2) Ebner, A. D.; Stanley, A. L.; Kaminski, M. D.; Rosengart, A. J.; Ritter, J. A. In *Theoretical Analysis of Ferromagnetic Seeding for Magnetic Drug Targeting*, Fifth International Conference on the Scientific and Clinical Applications of Magnetic Carriers, Lyon, France, 2004; The Cleveland Clinic Foundation: Lyon, France, 2004; p 39.

(3) Schopf, B.; Neuberger, T.; Schulze, K.; Petri, A.; Chastellain, M.; Steitz, B.; Hofmann, M.; Hofmann, H.; Rechenberg, B. v. In *Biocompatibility, tissue reaction, cellular uptake and detection of coated and functionalized superparamagnetic iron oxide nanoparticles (SPION) in cells of the musculoskeletal system*, Fifth International Conference on the Scientific and Clinical Applications of Magnetic Carriers, Lyon, France, 2004; The Cleveland Clinic Foundation: Lyon, France, 2004; p 26.

(4) Kaminski, M. D.; Rosengart, A. J.; Mertz, C. J.; Guy, S. G.; Xie, Y.; Chen, H.; Finck, M. R.; Balasubramanian, V.; Caviness, P. L. In *Functionalized Magnetic Nanospheres for Selective Removal of Blood-Born Toxins II: Preliminary Data*, Fifth International Conference on the Scientific and Clinical Applications of Magnetic Carriers, Lyon, France, 2004; The Cleveland Clinic Foundation: Lyon, France, 2004; p 83.

(5) Rosengart, A. J.; Kaminski, M. D.; Mertz, C. J.; Guy, S. G.; Xie, Y.; Chen, H.; Finck, M. R.; Caviness, P. L. In *Functionalized Magnetic Nanospheres for Selective Removal of Blood-Born Toxins I: Introduction and Initial Approach*, Fifth International Conference on the Scientific and Clinical Applications of Magnetic Carriers, Lyon, France, 2004; The Cleveland Clinic Foundation: Lyon, France, 2004; p 82.

(6) Plank, C.; Schillinger, U.; Brill, T.; Rudolph, C.; Huth, S.; Gersting, S.; Kroetz, F.; Hirschberger, J.; Bergemann, C. In *Advances in Magnetofection-magnetically guided nucleic acid delivery*, Fifth International Conference on the Scientific and Clinical Applications of Magnetic Carriers, Lyon, France, 2004; The Cleveland Clinic Foundation: Lyon, France, 2004; p 43.

(7) Reszka, R. C.; Martens, M.; Schueller, D. In *Magnetosome-Lipid/DNA-Complexes: a gene delivery and monitoring system of the next generation*, Fifth International Conference on the Scientific and Clinical Applications of Magnetic Carriers, Lyon, France, 2004; The Cleveland Clinic Foundation: Lyon, France, 2004; p 44.

(8) Jordan, A. In *First Clinical Experience with Magnetic Fluid Hyperthermia (MFH) at the University Clinic Charite in Berlin, Germany*, Fifth International Conference on the Scientific and Clinical Applications of Magnetic Carriers, Lyon, France, 2004; The Cleveland Clinic Foundation: Lyon, France, 2004; p 45.

10.1021/cm051346h CCC: $33.50
Published on Web 04/29/2006

synthesis of fullerene materials.[9−15] The resulting materials are reported to be oxidatively stable and chemically resistant, which are desirable qualities if such materials were to be used for biomedical applications. Harris et al. reported on the impregnation of a pyrolyzed block copolymer comprised of poly(vinylidene chloride) and poly(vinyl chloride) with a cobalt nitrate solution heated at 1800 °C for 2 h. Their findings indicated that a small percentage (5%) of metallic cobalt particles were encapsulated in graphite shells.[16] Tomita et al. reported that the transition metals (Co, Ni, and Fe) act as catalysts in graphitization and their studies revealed the beginning of a graphitic coating at 600 °C upon the annealing of cobalt and diamond particles with electron beam radiation.[17] Yudasaka et al. studied the properties of nickel films deposited on various allotropic carbon films. They concluded that nickel can catalyze the formation of graphite from any organic precursor; however, the organic precursor governs the temperature at which graphitization occurs.[18]

Herein, we report on the physical properties of cobalt nanoparticles prepared by the thermolysis of dicobalt octacarbonyl in poly(styrene-*b*-4-vinylphenoxyphthalonitrile) copolymer micelles and subsequently heated at 700 °C to create graphite-coated oxidatively stable cobalt nanoparticles. Magnetic susceptometry, transmission electron microscopy, electron diffraction, X-ray diffraction, and small-angle X-ray scattering techniques were used to assess the properties of these materials.

Experimental Section

Synthesis of Poly(styrene-*b*-4-vinylphenoxyphthalonitrile). A detailed synthetic procedure for poly(styrene-*b*-4-vinylphenoxyphthalonitrile) and the characterization thereof has been previously reported.[19] Briefly, the block copolymer was synthesized by a living anionic polymerization. First, poly(styrene-*b*-*tert*-butyldimethylsilyloxystyrene) was prepared by the sequential addition of styrene and *tert*-butyldimethylsilyloxystyrene monomers using *n*-butyllithium as the initiator. Next, the *tert*-butyldimethylsilyl ether group of poly(styrene-*b*-*tert*-butyldimethylsilyloxystyrene) was hydrolyzed under acidic conditions to generate poly(styrene-*b*-4-vinylphenol). Finally, poly(styrene-*b*-4-vinylphenoxyphthalonitrile) was synthesized by reacting 4-nitrophthalonitrile with poly(styrene-*b*-4-vinylphenol) in the presence of potassium carbonate. The resulting poly(styrene-*b*-4-vinylphenoxyphthalonitrile) polymer synthesized for this study had well-controlled block lengths of 50000 and 10000 g mol^{-1}, respectively (Figure 1). The polymers were thoroughly characterized with ^{1}H NMR, gel permeation chromatography (GPC), and infrared spectroscopy (IR).

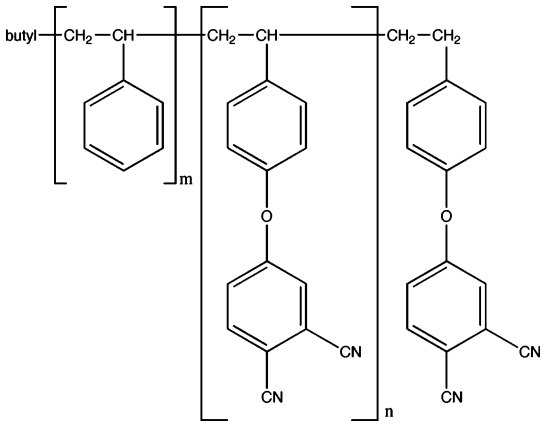

Figure 1. Poly(styrene-*b*-4-vinylphenoxyphthalonitrile).

Cobalt Nanoparticle Synthesis. Cobalt nanoparticles were synthesized by the addition of 1 g of dicobalt octacarbonyl into a reaction vessel containing 0.5 g of poly(styrene-*b*-4-vinylphenoxyphthalonitrile) dissolved in 50 mL of deoxygenated toluene. The reaction was refluxed at 110 °C for 5 h and the subsequent reaction product was placed into a capped vial and purged with dry nitrogen. Toluene was removed from the sample under vacuum at 100 °C for ∼24 h (pre-heat-treated sample).

Elevated Heat Treatment of Polymer-Coated Cobalt Nanoparticles. Approximately 1 g of the dried cobalt−polymer complex was placed into a ceramic boat and positioned in the center of a quartz tube furnace under a constant argon flow. The tube furnace was then heated at 700 °C for 4 h, after which the sample was removed and stored under atmospheric conditions for analysis (heat-treated sample).

Transmission Electron Microscopy. Transmission electron microscopy (TEM), high-resolution TEM (HRTEM), energy-filtered TEM (EFTEM), selected area electron diffraction (SAD), and nanobeam electron diffraction (NBD) were conducted with a JEOL 3000F field-emission transmission electron microscope (operated at 300 kV) equipped with a Gatan image filter (GIF) and digital imaging system. The pre-heat-treated sample was re-dispersed in toluene and cast onto an amorphous carbon-coated copper grid for analysis. The heat-treated sample was embedded in resin and microtomed to a thickness of ∼100 nm. Microtomed slices were then placed onto an amorphous carbon-coated copper grid for analysis. NBD was conducted on single crystals of the heat-treated sample using an ∼2 nm focused electron beam. Particle size analysis was performed on two fields of view for each sample. Each field of view was divided into sections and all of the particles of a particular section were measured in two directions: (1) in any obvious long direction and (2) perpendicular to the first measurement. The two measurements for each particle were then averaged and the aspect ratio for each particle (longer measurement/shorter measurement) was calculated. The mean and standard deviation were calculated for the particle size and aspect ratio for both fields of view of each sample. Energy-filtered TEM was conducted using the GIF with a spectrometer slit width of 40 eV at the cobalt $L_{3,2}$ edge (778−793 eV). Pre-edge background images were acquired at 714 and 753 eV and the post-edge image at 799 eV.

Small-Angle X-ray Scattering. Small-angle X-ray scattering (SAXS) measurements were conducted on a Bruker Nanostar SAXS instrument. Samples were prepared by placing a powdered fraction of each sample in the center of a sample holder where it was held in place with adhesive tape. The samples were measured for 12 h over a 2θ range of 0−4.4° with a Cu K_α source.

X-ray Diffraction. Siemens X-ray diffractometers (model D-500 for the pre-heat-treated sample and D-5000 for the heat-treated

(9) Host, J. J.; Block, J. A.; Parvin, K.; Dravid, V. P.; Alpers, J. L.; Sezen, T.; LaDuca, R. *J. Appl. Phys.* **1998**, *83* (2), 793.
(10) Jiao, J.; Seraphin, S.; Wang, X.; Withers, J. C. *J. Appl. Phys.* **1996**, *80* (1), 103.
(11) McHenry, M. E.; Majetich, S. A.; Artman, J. O.; DeGraef, M.; Staley, S. W. *Phys. Rev. B* **1994**, *49* (16), 11 358.
(12) Chen, C. P.; Chang, T. H.; Wang, T. F. *Ceram. Int.* **2001**, *27*, 925.
(13) Seraphin, S.; Zhou, D.; Jiao, J. *J. Appl. Phys.* **1996**, *80* (4), 2097.
(14) Saito, Y.; Masuda, M. *Jpn. J. Appl. Phys.* **1995**, *34*, 5594.
(15) Saito, Y. *Carbon* **1995**, *33* (7), 979.
(16) Harris, P. J. F.; Tsang, S. C. *Chem. Phys. Lett.* **1998**, *293*, 53.
(17) Tomita, S.; Hikita, M.; Fujii, M.; Hayashi, S.; Yamamoto, K. *Chem. Phys. Lett.* **2000**, *316*, 361.
(18) Yudasaka, M.; Tasaka, K.; Kikuchi, R.; Ohki, Y.; Yoshimura, S. *J. Appl. Phys.* **1997**, *81* (11), 7623.
(19) Baranauskas, V. V.; Zalich, M. A.; Saunders: M.; St. Pierre, T. G.; Riffle, J. S. *Chem. Mater.* **2005**, *17*, 5246.

sample, both using Cu K_α radiation) were used to acquire X-ray diffraction patterns of the pre-heat-treated and heat-treated samples. Powdered samples were placed onto polycarbonate sample holders and scanned at (1) a rate of 0.2°/min with a step size of 0.03° from 10 to 110° for the pre-heat-treated sample and (2) a rate of 0.13 °/min with a step size of 0.04° from 10 to 110° for the heat-treated sample. Cobalt nanocrystal size for each sample was estimated using the Scherrer equation.

Magnetic Susceptometry. A Quantum Design magnetic properties measurement system (MPMS-7) equipped with a superconducting quantum interference device (SQUID)-based sensor was used to make cobalt-specific magnetization measurements (σ) at varying applied fields (H) from −70000 to +70000 Oe at 300 and 5 K, with 100 Oe spacings between −1000 and 1000 Oe. Low-temperature measurements were conducted both after the sample was cooled in zero applied field and in an applied field of 70000 Oe. The purpose of the different measurements was to study (1) the saturation magnetization at 300 K, (2) the hysteretic behavior of the sample at 300 K, (3) the presence of an exchange bias, owing to a cobalt oxide layer on the surface of the cobalt nanoparticles, and (4) the presence of paramagnetic species, owing to any residual cobalt carbonyl species in the sample. In addition, isothermal remanent magnetization (IRM) and dc-demagnetization (DCD) curves were generated at 300 K in order to qualitatively understand the interparticle interactions of the magnetic cobalt nanoparticles in both systems. The IRM curve was measured by applying a constant magnetic field for 700 s, removing the field and measuring the remanent moment 700 s after field removal. This process was conducted up to 20 kOe (in 500 Oe steps), whereupon the procedure was reversed (beginning at −500 Oe) and followed by applying negative fields to −20 kOe to provide the DCD curve. Henkel plots generated from these data were constructed by plotting the normalized IRM remanence vs DCD remanence magnetizations.

Elemental Analysis. Elemental analyses were performed on the pre-heat-treated and heat-treated samples using inductively coupled plasma atomic emission spectroscopy (ICP-AES) at the Marine and Freshwater Research Laboratory at Murdoch University, Perth, Western Australia. The samples were prepared by digestion in a 1:1 mixture of HNO_3:H_2SO_4 for 13 days at 70−100 °C. The samples and a blank were diluted and analyzed for cobalt concentrations.

Results and Discussion

Particle Analysis. Transmission electron microscopy (TEM) was used to study the particle size, size distribution, morphology, chemical composition, and crystallinity of the pre-heat-treated and heat-treated cobalt complexes. A "particle" was deemed to be a region with contrast obviously different from the background. Diffraction contrast causes individual particles to have different intensities. Particles were easy to define in the heat-treated sample due to the strong crystallinity and contrast relative to the background and the relatively large particle size. The decreased crystallinity and smaller particle size of the pre-heat-treated sample made it more difficult to accurately identify the edges of the particles and more care was needed to ensure that accurate particle size data were obtained in this case. Others have also observed the crytallization of magnetic metals upon heat treatment. Koltypin and co-workers and Rojas and co-workers performed in situ TEM heating studies (at 500 and 600 °C) on pre-heat-treated Ni nanomaterials and observed the formation of Ni nanoparticles from Ni atoms, confirming that heat treatment induces Ni crystallization.[20,21]

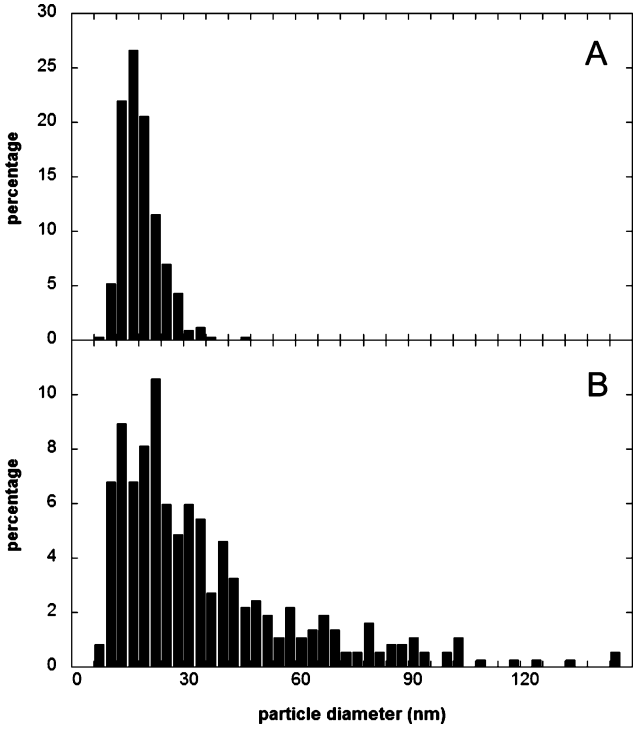

Figure 2. Particle size histograms for (A) pre-heat-treated and (B) heat-treated samples.

The particle size distribution for the pre-heat-treated sample ranged from 9 to 45 nm with a mean of 18.5 nm (sample population = 346 particles) (Figure 2). The average aspect ratio for particles of the pre-heat-treated sample was 1.43 with a standard deviation of 0.39. A dramatic increase in particle size and size distribution after heat treatment at 700 °C was apparent from the images taken during analysis. The particle size distribution for the heat-treated sample increased from 7 to 147 nm with a mean of 36.1 nm (sample population = 369 particles) (Figure 2). The average aspect ratio was 1.48 with a standard deviation of 0.51. These increases in mean particle size and size distribution are likely to be due to particle sintering at 700 °C, which may be explained by an Ostwald ripening mechanism similar to that reported by Host et al.[9]

Small-Angle X-ray Scattering. Small-angle X-ray scattering data were analyzed using Igor Pro (Wavemetrics) software and a NIST subroutine (PolyCoreForm)[22] modeling X-ray scattering from polydisperse spheres. Mean particle size values and standard deviations determined from TEM were entered as starting values for the fitting. Three additional fits of models to the data were evaluated, where the particle size, polydispersity, and particle size/polydispersity values were permitted to vary to optimize the curve fitting (curves not shown). The measured SAXS data were consistent with the particle size and size distribution data obtained from TEM particle size analysis. The SAXS data indicated

(20) Rojas, T. C.; Sayagues, M. J.; Caballero, A.; Koltypin, Y.; Gedanken, A.; Ponsonnet, L.; Vacher, B.; Martin, J. M.; Fernandez, A. *J. Mater. Chem.* **2000**, *10*, 715.
(21) Koltypin, Y.; Fernandez, A.; Rojas, T. C.; Campora, J.; Palma, P.; Prozorov, R.; Gedanken, A. *Chem. Mater.* **1999**, *11*, 1331.
(22) NIST. *SANS Analysis with Igor Pro*, http://www.ncnr.nist.gov/programs/sans/manuals/data_anal.html, Feb 28, 2005.

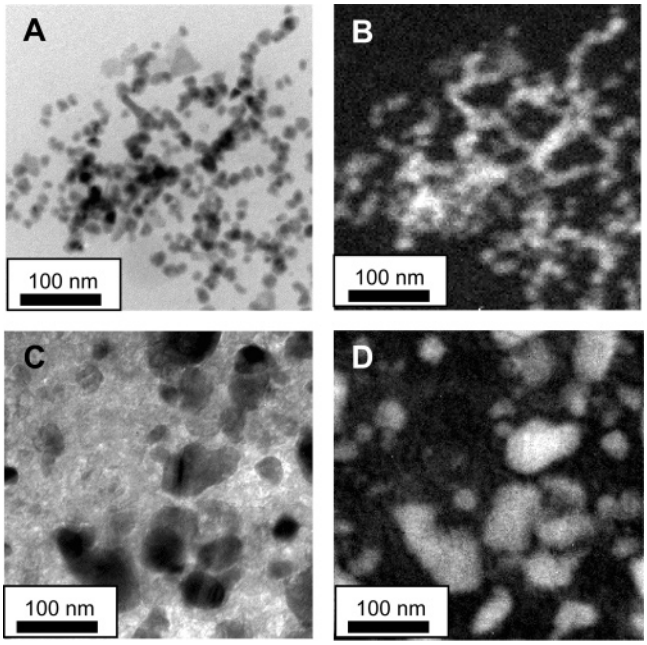

Figure 3. (A) Bright-field image of pre-heat-treated sample, (B) corresponding cobalt distribution image of (A), (C) bright-field image of heat-treated sample, and (D) corresponding cobalt distribution image of (C).

that the pre-heat-treated sample comprised smaller particles with a narrower size distribution than the heat-treated sample.

Transmission Electron Microscopy. Energy-filtered TEM (EFTEM) was conducted on the pre-heat-treated and heat-treated samples to confirm the elemental identity of the electron dense nanoparticles. The resulting cobalt distribution maps correlated well with the electron dense regions of the bright field images, confirming the chemical identity of the particles in both samples (Figure 3).

There are two reported phases of cobalt for nanomaterials: (1) face-centered cubic (fcc)[23,24] and (2) epsilon (ϵ).[25−27] Moreover, the three reported phases of cobalt (hexagonal close packed (hcp), fcc, and ϵ) are very close in energy and low activation energies are sufficient to cause stacking faults and possibly complete phase transitions.[25,26]

High-resolution TEM (HRTEM) was used to observe the presence of any crystallinity in the cobalt nanoparticles. HRTEM analysis of the pre-heat-treated sample indicated weak particle crystallinity; however, there were some well-crystallized particles (Figure 4A). Measurements of planar spacings (1.97 Å) from an exemplary highly crystalline particle are consistent with the {111} crystal plane (2.05 Å) of fcc cobalt, but could also correspond to the {002} or {101} crystal plane of hcp cobalt or the {310} crystal plane of ϵ cobalt (2.04 Å).[25,28,29]

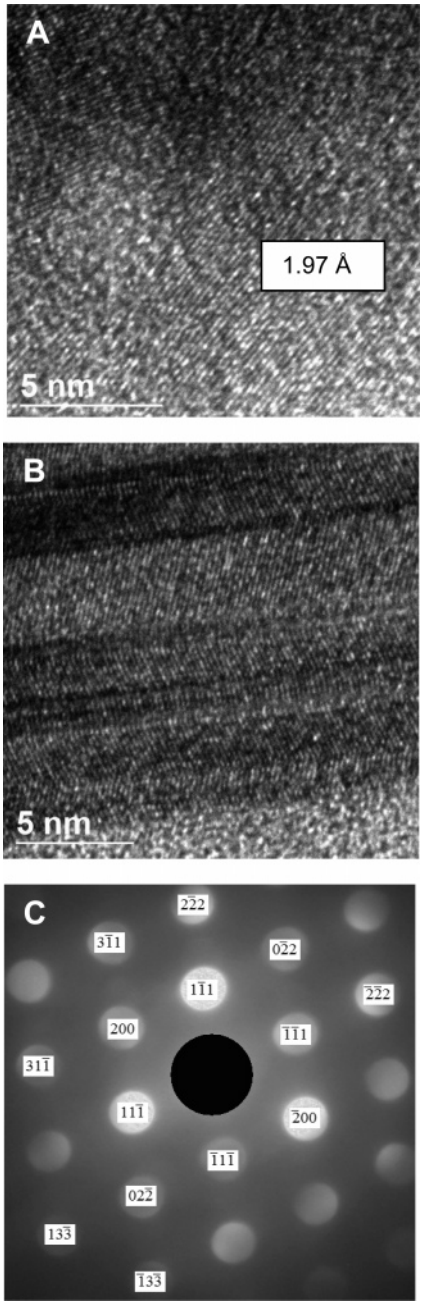

Figure 4. (A) HRTEM of pre-heat-treated sample, (B) HRTEM of heat-treated sample showing multiple twinning within a single crystal, and (C) indexed nanobeam electron diffraction pattern of ⟨011⟩ zone axis of fcc cobalt.

HRTEM of the heat-treated sample revealed highly crystalline particles with defects, such as twin planes. Twinning is commonly observed in nanocrystals, often among fcc materials.[30] Measurements of lattice spacings (2.04 Å) of a multi-twinned crystalline particle again matched the {111} plane of fcc cobalt (2.05 Å) (Figure 4B). The presence of fcc cobalt was confirmed through nano-beam electron diffraction of individual particles (Figure 4C). A small number of particles demonstrating hcp structure were also found (Figure 5A). A Fourier transform of Figure 5A gives a hexagonal arrangement of spots at a 2.2 Å spacing, consistent with the $\{10\bar{1}0\}$ plane in hcp-Co (Figure 5B). In

(23) Gubin, S. P.; Spichkin, Y. I.; Koksharov, Y. A.; Yurkov, G. Y.; Kozinkin, A. V.; Nedoseikina, T. I.; Korobov, M. S.; Tishin, A. M. *J. Magn. Magn. Mater.* **2003**, *265*, 234.
(24) Park, J.; Kang, N.; Jun, Y.; Oh, S. J.; Ri, H.; Cheon, J. *Chem. Phys. Chem.* **2002**, *6*, 543.
(25) Dinenga, D. P.; Bawendi, M. G. *Angew. Chem., Int. Ed.* **1999**, *38* (12), 1788.
(26) Puntes, V. F.; Krishnan, K. M.; Alivisatos, A. P. *Science* **2001**, *291*, 2115.
(27) Sun, S.; Murray, C. B. *J. Appl. Phys.* **1999**, *85* (8), 4325.
(28) Cobalt, F. C. C. In *JCPDS-International Centre for Diffraction Data*; card 15-0806, 1996.
(29) Cobalt, H. C. P. In *JCPDS-International Centre for Diffraction Data*; card 05-0727, 1996.
(30) Wang, J.; Tian, M.; Mallouk, T. E.; Chan, M. H. W. *J. Phys. Chem. B* **2004**, *108*, 841.

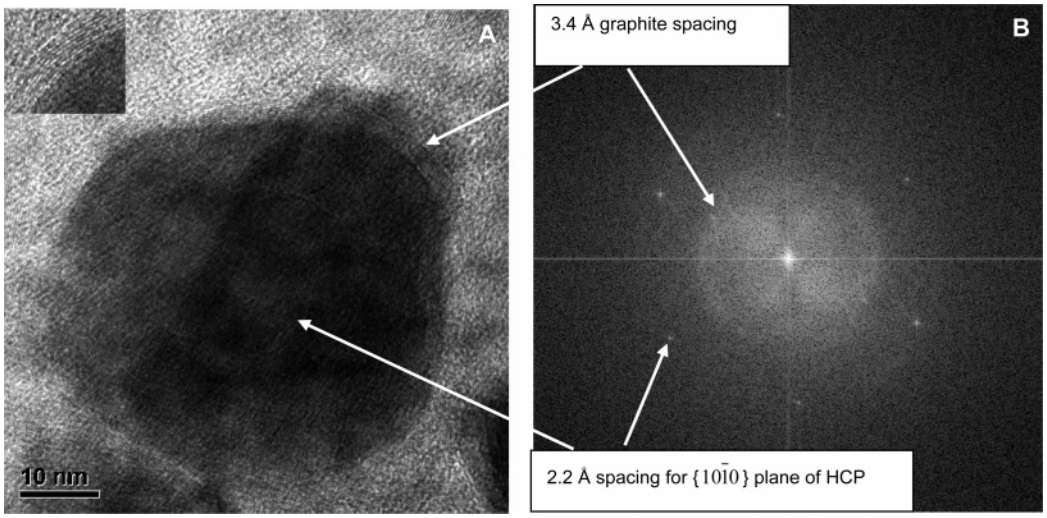

Figure 5. (A) High-resolution image of hcp cobalt particle and (B) Fourier transform of A showing graphite and hcp spacings. Inset in A is a magnified region of graphitic layers.

addition, the high-resolution image revealed the presence of a graphitic coating around the cobalt particle (Figure 5A inset). Measurements of the Fourier transform of Figure 5A indicated that the spacing between the layers surrounding the particle is consistent with the interlayer spacing of graphite (3.4 Å).[31] This graphitic coating may be the barrier that afforded the observed oxidation protection for over 1 year.[19] It is not clear from the HRTEM images whether the particle coatings are uniform (Figure 5A). This may be attributed to particle orientation with respect to the incident electron beam and may also be complicated by some overlapping particles. However, the X-ray diffraction peak at $2\theta \sim 24°$ for the heat-treated material suggests that a large population of the particles have a graphitic coating. These data are discussed further in the following section. McHenry et al. also reported the presence of faulted graphite-coated cobalt particles prepared by a process based on the Krätschmer−Huffman carbon arc process.[11]

X-ray Diffraction. X-ray diffraction (XRD) was used to complement electron diffraction data as it provides crystallographic information on the bulk of the sample in an effort to determine the presence of a dominant phase of cobalt in these systems. Broad peaks at $2\theta = 17°$ were found in both diffraction patterns and are due to an adhesive used to hold the samples on the holder. XRD yielded information about the crystal phase of cobalt in the pre-heat-treated sample, despite its weakly crystalline nature. With use of the JCPDS database, the structure was determined to be fcc cobalt (Figure 6 top, Table 1), although there were other peaks (a and b) that appeared in the diffraction pattern. These peaks seemed to match well with cobalt oxide, which is likely since the magnetic susceptometry measurements indicated a cobalt oxide component in the pre-heat-treated sample (see Magnetometry section). XRD also clarified the crystal phase of cobalt in the heat-treated sample. The peaks in the heat-treated sample diffraction pattern were more well-defined than the pre-heat-treated sample, indicating that an improvement in crystallinity had taken place during the heating procedure (Figure 6 bottom). Furthermore, the peaks were matched to the fcc phase of cobalt using the JCPDS software database (Table 2). Thus, it appears that the dominant phase of cobalt in the heat-treated cobalt nanoparticle system is fcc; however, there may be a small percentage of hcp and ϵ-cobalt present. Saito and Masuda and Saito reported that small amounts of the hcp phase of cobalt were formed by a method based on the carbon arc method for fullerene production; however, the dominant phase was fcc cobalt.[14,15] Additionally, the broad peak at $2\theta \approx 24°$ corresponds to an experimental d spacing of 3.7 Å. This value falls within the range reported for the interplanar spacings of graphite ($d_{002} = 3.4-3.9$ Å) in carbon nanotubes of varying diameter.[31] Since the peak is broad, it is thought to encompass graphitic spacings of coatings on particles of varying dimensions. Finally, the Scherrer equation was used to examine peak broadening caused by differences in nanocrystallite size. The X-ray diffraction peaks were broader for the pre-heat-treated sample and calculations using the Scherrer equation indicated an average crystallite size of 5.2 nm. The X-ray diffraction peaks were narrower for the heat-treated sample, and calculations indicated an average crystallite size of 17.5 nm. These data suggest that cobalt nanocrystallite size increases during heat treatment at 700 °C, which is consistent with both TEM and SAXS data on the particle sizes of these systems.

Magnetic Susceptometry. Magnetic susceptometry measurements were conducted on the pre-heat-treated and heat-treated samples at 300 and 5 K to elucidate their magnetic properties. Room temperature σ vs H measurements of the pre-heat-treated sample revealed a cobalt-specific saturation magnetization (σ_s) of 81 emu g^{-1} Co, remanent magnetization (M_r) of 19 emu g^{-1} Co, and a coercivity (H_c) of ~410 Oe (Figure 7A). The magnetic remanence and coercivity values along with zero field cooled/field cooled σ vs T measurements indicated that the sample is comprised of a combination of superparamagnetic and magnetically blocked particles at room temperature.

The slope of the magnetization curve is positive in high fields at low temperature, while at 300 K this slope is reduced and the magnetization curve almost saturates at high fields

(31) Kiang, C. H.; Endo, M.; Ajayan, P. M.; Dresselhaus, G.; Dresselhaus, M. S. *Phys. Rev. Lett.* **1998**, *81* (9), 1869.

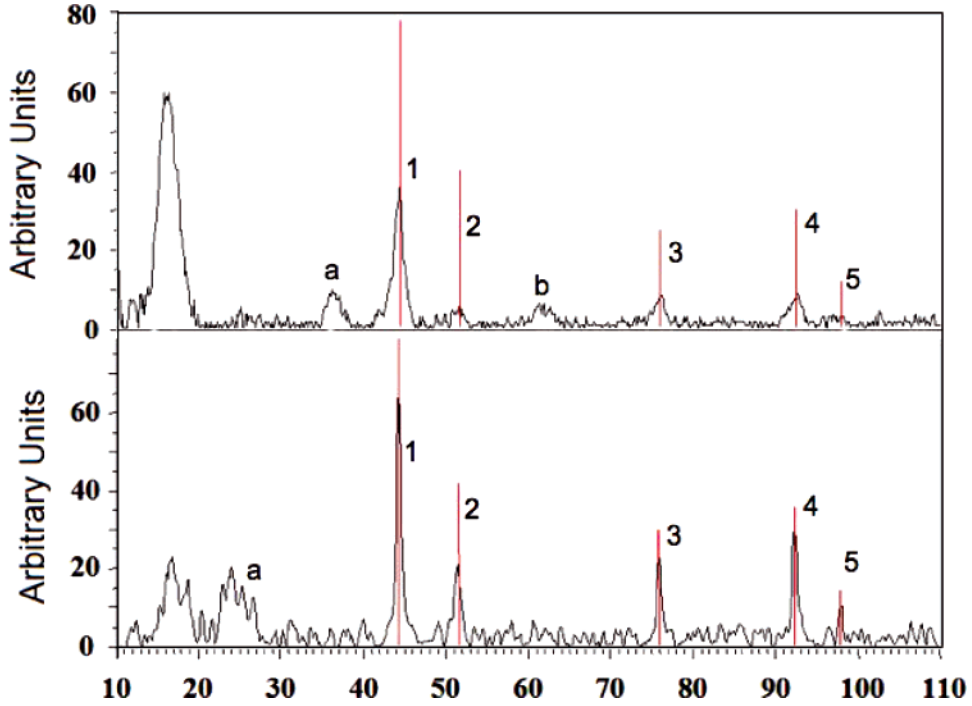

Figure 6. X-ray diffraction patterns for pre-heat-treated sample (top) and heat-treated sample (bottom). Vertical lines are peak matches provided by the JCPDS software database.

Table 1. Experimental and Literature *d* Spacings for fcc Cobalt for the Pre-heat-treated Sample

peak number	2θ	*d* spacing in Å (experimental)	*d* spacing in Å (literature)
1	44.24	2.05	2.05
2	51.49	1.78	1.77
3	75.88	1.25	1.25
4	92.38	1.07	1.07
5	97.84	1.02	1.02
a (Co_3O_4)	36.16	2.48	2.44
b (CoO)	61.69	1.50	1.51

Table 2. Experimental and Literature *d* Spacings for fcc Cobalt for the Heat-treated Sample

peak number	2θ	*d* spacing in Å (experimental)	*d* spacing in Å (literature)
1	44.24	2.05	2.05
2	51.52	1.77	1.77
3	75.84	1.25	1.25
4	92.28	1.07	1.07
5	98.12	1.02	1.02
a	24.08	3.70	3.4−3.9[31]

(Figure 7). This positive slope at 5 K is indicative of the presence of paramagnetic material with a possible contribution from an antiferromagnetic component in the sample. It is difficult to separate the paramagnetic component from the antiferromagnetic component, as the magnitude of their effects is similar, but much lower than that of a ferromagnetic material. The paramagnetic component may be due to unreacted cobalt carbonyl species that have not been incorporated into cobalt nanoparticles. Low-temperature zero field cooled/field cooled hysteresis loop experiments exhibit an asymmetric field cooled hysteresis loop shift. This field cooled hysteresis loop shift is indicative of an exchange bias ($H_e \approx 3200$ Oe) created by the coupling of an antiferromagnetic cobalt oxide surface layer with the ferromagnetic cobalt metal core.[32−34] Thus, the departure of σ_s for the pre-heat-treated sample from the value for bulk cobalt is most likely due to residual cobalt carbonyl species and the partial oxidation of the sample.

Two different sample digestion procedures led to two different cobalt concentration measurement results for the heat-treated sample as reported by Baranauskas et al.[19] Briefly, the first digestion procedure involved dissolving the sample in a 1:1 mixture of concentrated HNO_3:H_2SO_4 for 4 days between 70 and 100 °C. The second procedure involved dissolving the sample in a 1:1 mixture of concentrated HNO_3:H_2SO_4 for 13 days between 70 and 100 °C with an addition of 5 mL of concentrated H_2SO_4 on the ninth day. The relatively robust nature of a protective graphitic coating will hamper acid digestion of the metallic cobalt and hence is likely the cause for disagreement between the elemental analysis data. The first digestion procedure (D1) gave a [Co] = 31% by mass while the more rigorous second digestion procedure (D2) gave a [Co] = 41% by mass. The difference in these cobalt concentrations suggests that (1) the protective coating can be digested over time under extreme conditions or (2) it takes a significant amount of time for the acid to penetrate defects in the graphitic coatings and dissolve the cobalt particles. Room-temperature magnetic susceptometry measurements showed apparent saturation magnetizations of 230 emu g^{-1} of calculated Co for D1 and 172 emu g^{-1} of calculated cobalt for D2 (Figure 8A). Both the magnitude of these values and their differences indicate that the sample digestion procedure for this material is critical to the values of cobalt concentration obtained from the ICP-AES measurements. The value of 230 emu g^{-1} Co for D1 is significantly higher than the maximum cobalt-specific magnetization expected based on the value for bulk cobalt, and hence implies that the sample digestion was incomplete. The

(32) Berkowitz, A. E.; Takano, K. *J. Magn. Magn. Mater.* **1999**, *200*, 552.
(33) Kiwi, M. *J. Magn. Magn. Mater.* **2001**, *234*, 584.
(34) Nogues, J.; Schuller, I. K. *J. Magn. Magn. Mater.* **1999**, *192*, 203.

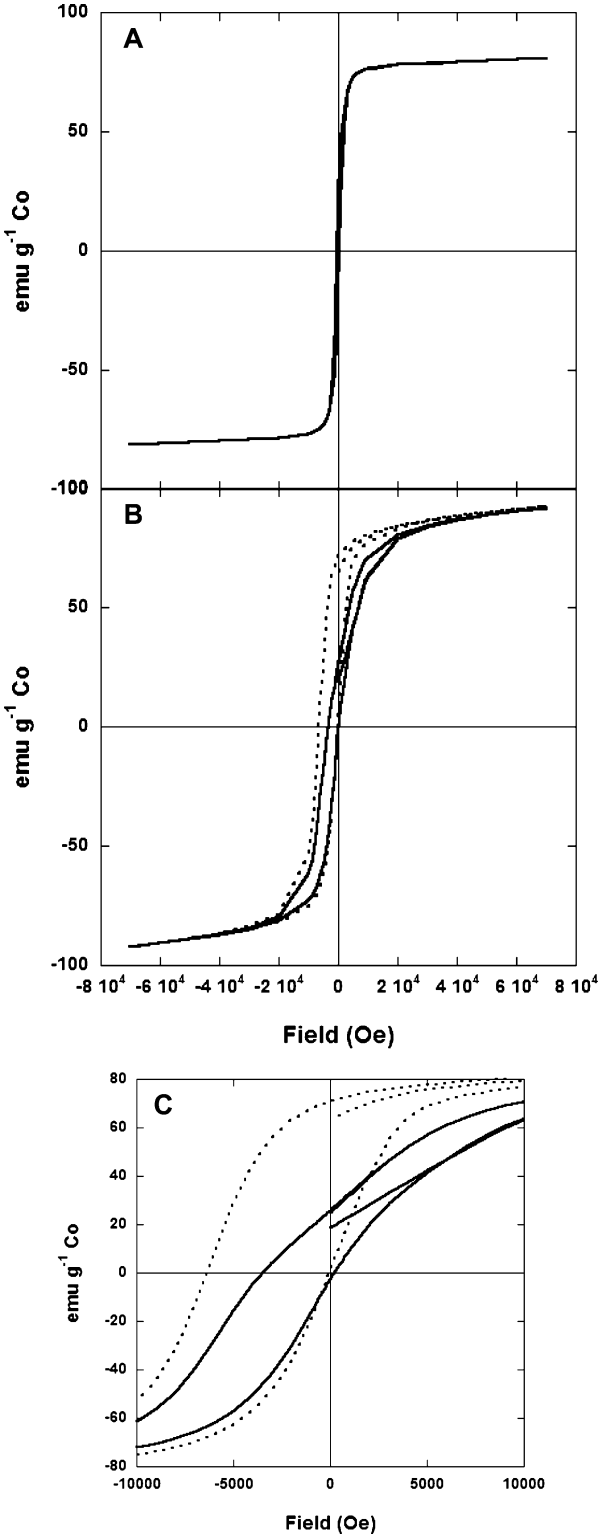

Figure 7. σ vs H measurements conducted at (A) 300 K and (B) 5 K (zero field cooled hysteresis loop, —; field cooled hysteresis loop, ···) on pre-heat-treated cobalt−polymer complexes that had been aged under ambient conditions for 3 months. (C) shows the enlarged region around the origin for 5 K hysteresis loops showing the asymmetric field cooled hysteresis loop shift.

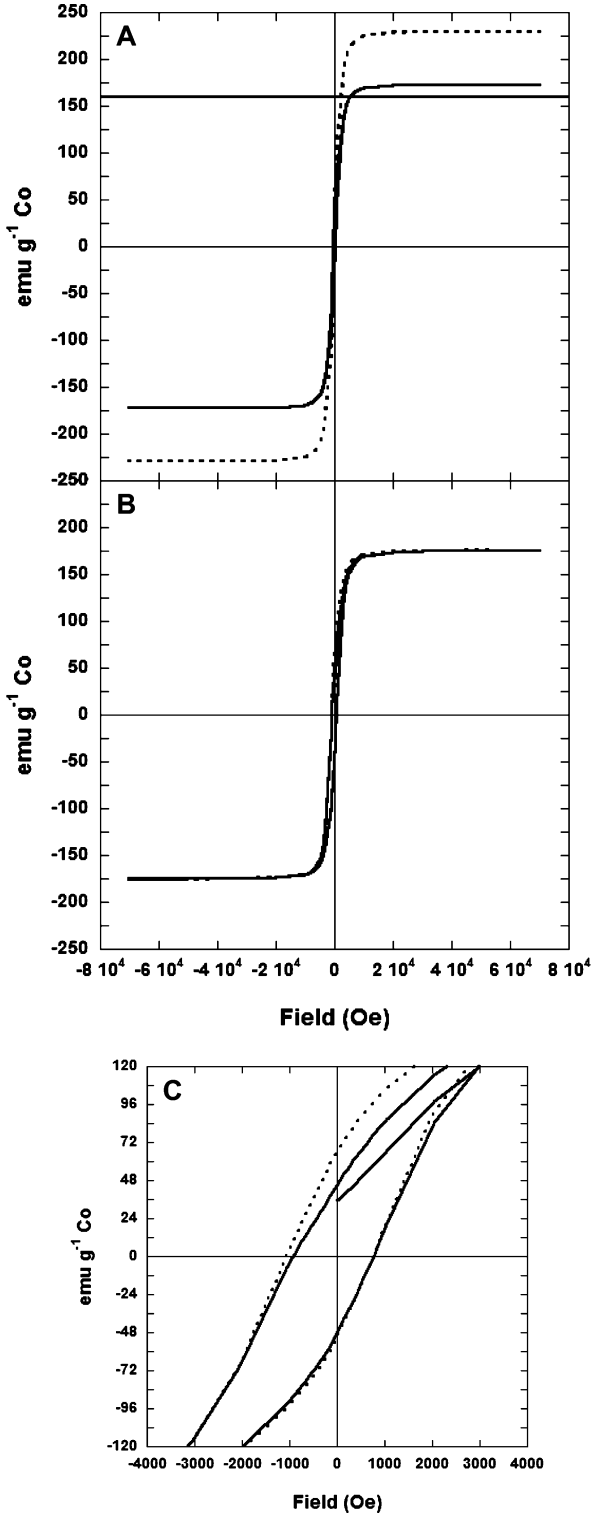

Figure 8. σ vs H measurements conducted on a cobalt−copolymer sample that had been thermally treated at 700 °C at (A) 300 K (4 day acid digestion (···) and 13 day acid digestion (—)) and (B) 5 K (13 day acid digestion: zero field cooled (—), field cooled (···)). (C) shows the enlarged region around the origin for 5 K hysteresis loops (13 day acid digestion) and shows minimal field cooled hysteresis loop shift. The horizontal line at 160 emu g^{-1} Co in (A) indicates the maximum reported specific magnetization for cobalt metal.

reduction in the apparent cobalt-specific magnetization with increased digestion time suggests that the digestion process is very slow for this material. Several research groups have investigated the use of acid digestion techniques to dissolve unencapsulated cobalt formed when preparing graphite-coated cobalt nanoparticles using a modified arc-discharge procedure. Their findings indicated that cobalt particles completely encapsulated by graphite were not dissolved; however, the acid treatments used were not as rigorous as reported above.[10,13,35] It is reasonable that strong mineral acids will eventually penetrate minor defects in the graphite

coatings, leading to cobalt dissolution. Moreover, the difference of σ_s for D2 (172 emu g^{-1} Co) is only 7.5% larger than the literature value of ~160 emu g^{-1} Co.[36] This error may be within the limits of reproducibility for the elemental analysis measurements. Kobayashi et al. studied the magnetic properties of silica-coated cobalt nanoparticles heated for 2 h at temperatures ranging from 200 to 700 °C in air. The cobalt-specific saturation magnetization of their materials heated at 700 °C was zero, while the cobalt-specific saturation magnetizations for the 700 °C heat-treated materials described in this manuscript were similar to those of bulk cobalt. The heat treatment of the silica-coated cobalt materials in air, as opposed to heating in an inert atmosphere, may have led to the formation of amorphous and crystalline cobalt oxide as evidenced by (1) the decrease in M_s with increasing treatment temperature (500 to 700 °C) and (2) the appearance of cobalt oxide peaks and disappearance of cobalt peaks in the X-ray diffraction patterns.[37] Room-temperature magnetic hysteresis loop measurements showed that the sample exhibits magnetic remanence and coercivity (M_r = 34 emu g^{-1} Co; H_c = 416 Oe). Field cooled and zero field cooled σ vs T measurements in conjunction with σ vs H measurements at room temperature (Figure 8A) suggest that the heat-treated sample consists of a combination of particles that are superparamagnetic and magnetically blocked at room temperature.

Low-temperature magnetization measurements on these heat-treated cobalt−graphitic complexes indicate similar saturation magnetizations to those measured at room temperature. Field cooled σ vs H measurements show magnetic hysteresis with negligible field bias (H_e = 144 Oe) relative to zero field cooled σ vs H measurements (Figures 8B and 8C), suggesting the absence of cobalt oxide layers around the metallic cobalt nanoparticles. The long-term saturation magnetization stability confirms that the annealed carbonaceous cobalt complexes are oxidatively stable.[19] Compared with the pre-heat-treated sample, the cobalt-specific magnetization for the heat-treated sample saturates at high fields in both room-temperature and low-temperature studies, indicating an absence of the paramagnetic component that was observed for the pre-heat-treated sample. It is possible that residual carbonyl species evolve during thermal treatment with the concomitant incorporation of residual cobalt atoms into the cobalt nanoparticles, and that this largely decreases or eliminates any paramagnetic species in the sample.

Henkel plots (not shown) for the pre-heat-treated and heat-treated systems indicated weak interparticle demagnetizing magnetic interactions, as would be expected for magnetic cobalt nanoparticles in close proximity with each other (but not in direct contact).

Conclusions

Cobalt nanoparticles were prepared by the thermolysis of dicobalt octacarbonyl in poly(styrene-*b*-4-vinylphenoxyphthalonitrile) block copolymer micelles. The particles were subsequently heat-treated at 700 °C to afford oxidatively stable cobalt nanoparticles with a "graphitic" coating. The cobalt-specific saturation magnetization value increased upon heating due to one or both of the following reasons: (1) sintering of cobalt nanoparticles, leading to an increase in particle size; (2) annealing of cobalt nanoparticles, leading to an increase in particle crystallinity. A graphitic coating appears to be the protective barrier against oxidation for the heat-treated cobalt nanoparticles. Transmission electron microscopy, electron diffraction, and X-ray diffraction were used to identify the dominant crystal phase of the pre-heated and heat-treated samples as being face-centered cubic, although there may be oxide present in the pre-heated sample and other phases of cobalt (hcp, ϵ) present.

Future work will involve studying the heat treatment process in more detail to create an oxygen-impermeable coating around the cobalt nanoparticles and to improve the particle crystallinity without any particle sintering.

Acknowledgment. The authors of this paper acknowledge the support of NSF under Contract DMR-0312046, DARPA-AFOSR (Contracts #F49620-02-1-0408 and F49620-03-1-0332), OMNOVA Solutions and the Australian Research Council (Grant # DP0559333) for funding. We also are grateful for the support from NSF under Contract CHE-023488 for the funding to purchase a SQUID magnetometer used extensively for the research described herein. M. A. Zalich thanks the Australian-American Fulbright Commission for a Fulbright Postgraduate Fellowship to conduct research in Australia. The authors would also like to thank Dr. J. Connolly from Curtin University of Technology, Perth, Australia, for help with SAXS data acquisition and E. Bovell from The University of Western Australia for help with SAXS curve fitting.

CM051346H

(35) Host, J. J.; Teng, M. H.; Elliot, B. R.; Hwang, J.; Mason, T. O.; Johnson, D. L.; Dravid, V. P. *J. Mater. Res.* **1997**, *12* (5), 1268.
(36) Bozorth, R. M. *Ferromagnetism*, 5th ed.; D. Van Nostrand Company, Inc.: New York, 1959; p 968.
(37) Kobayashi, Y.; Horie, M.; Konno, M.; Rodriguez-Gonzalez, B.; Liz-Marzan, L. M. *J. Phys. Chem. B* **2003**, *107*, 7420.